Report

Cell Reports

Identification of a Paralog-Specific Notch1 Intracellular Domain Degron

Graphical Abstract

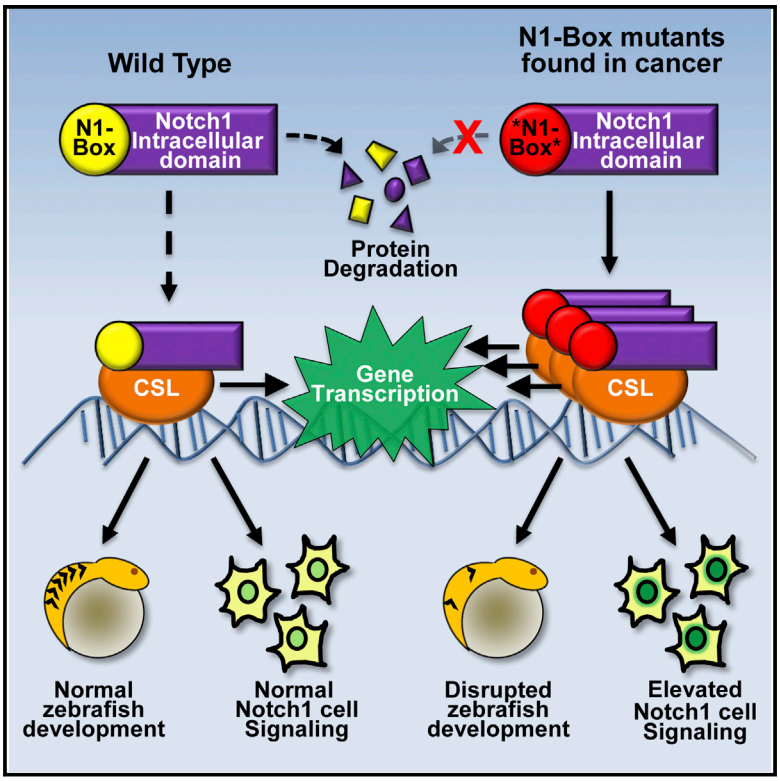

Highlights

- A biochemical assay identifies the N1-Box degron of the Notch1 intracellular domain
- Mutations in the Notch1 N1-Box promote signaling in human cells and zebrafish
- The N1-Box functions independently of other known Notch1 degrons
- Human cancer mutations within the N1-Box exhibit elevated Notch1 activity in vivo

Authors

Matthew R. Broadus, Tony W. Chen, Leif R. Neitzel, ..., James G. Patton, Stacey S. Huppert, Ethan Lee

Correspondence

stacey.huppert@cchmc.org (S.S.H.), ethan.lee@vanderbilt.edu (E.L.)

In Brief

Notch is essential for metazoan development and is mutated in human cancers. Broadus et al. identify a paralog-specific degron (N1-Box) that promotes degradation of the Notch1 intracellular domain, thereby limiting Notch1 pathway activity. Cancer mutations within the N1-Box exhibit enhanced Notch1 signaling in zebrafish, highlighting the importance of N1-Box in proper Notch1 signaling.

Broadus et al., 2016, Cell Reports *15*, 1920–1929
May 31, 2016
http://dx.doi.org/10.1016/j.celrep.2016.04.070

OPEN ACCESS
CellPress

Cell Reports
Report

Identification of a Paralog-Specific Notch1 Intracellular Domain Degron

Matthew R. Broadus,[1,2,9] Tony W. Chen,[1,9] Leif R. Neitzel,[1] Victoria H. Ng,[1] Jeanne N. Jodoin,[1,7] Laura A. Lee,[1] Adrian Salic,[2] David J. Robbins,[3,4] Anthony J. Capobianco,[3,4] James G. Patton,[5] Stacey S. Huppert,[6,10,*] and Ethan Lee[1,8,10,*]

[1]Department of Cell and Developmental Biology, Vanderbilt University Medical Center, Nashville, TN 37232, USA
[2]Department of Cell Biology, Harvard Medical School, Boston, MA 02115, USA
[3]Molecular Oncology Program, Division of Surgical Oncology, Dewitt Daughtry Family Department of Surgery
[4]Sylvester Comprehensive Cancer Center, Miller School of Medicine
University of Miami, Miami, FL 33136, USA
[5]Department of Biological Sciences, Vanderbilt University, Nashville, TN 37232, USA
[6]Division of Gastroenterology, Hepatology, and Nutrition, Cincinnati Children's Hospital Medical Center, Cincinnati, OH 45229, USA
[7]Department of Biology, Massachusetts Institute of Technology, Cambridge, MA 02142, USA
[8]Vanderbilt Ingram Cancer Center, Vanderbilt Medical Center, Nashville, TN 37232, USA
[9]Co-first author
[10]Co-senior author
*Correspondence: stacey.huppert@cchmc.org (S.S.H.), ethan.lee@vanderbilt.edu (E.L.)
http://dx.doi.org/10.1016/j.celrep.2016.04.070

SUMMARY

Upon Notch pathway activation, the receptor is cleaved to release the Notch intracellular domain (NICD), which translocates to the nucleus to activate gene transcription. Using *Xenopus* egg extracts, we have identified a Notch1-specific destruction signal (N1-Box). We show that mutations in the N1-Box inhibit NICD1 degradation and that the N1-Box is transferable for the promotion of degradation of heterologous proteins in *Xenopus* egg extracts and in cultured human cells. Mutation of the N1-Box enhances Notch1 activity in cultured human cells and zebrafish embryos. Human cancer mutations within the N1-Box enhance Notch1 signaling in transgenic zebrafish, highlighting the physiological relevance of this destruction signal. We find that binding of the Notch nuclear factor, CSL, to the N1-Box blocks NICD1 turnover. Our studies reveal a mechanism by which degradation of NICD1 is regulated by the N1-Box to minimize stochastic flux and to establish a threshold for Notch1 pathway activation.

INTRODUCTION

The Notch pathway is a highly conserved, metazoan signaling pathway critical for organismal development (Kopan and Ilagan, 2009). The Notch pathway communicates transcriptional decisions between adjacent cells through direct interaction of a Delta/Serrate/Lag-2 (DSL) type 1 transmembrane ligand on the signaling cell and a Notch type 1 transmembrane receptor on a receiving cell. This interaction promotes a series of proteolytic events resulting in liberation of the Notch intracellular domain (NICD) from its membrane tether. Liberated NICD enters the nucleus, where it forms a complex with CSL (CBF1/RBPjk/Su(H)/Lag-1), MAML (Mastermind-like), and CoA (coactivators) (Kovall and Blacklow, 2010). Formation of this complex drives transcription of Notch target genes. In the prevailing model, transcriptional termination is mediated, in part, by the E3 ubiquitin ligase complex, SCF^{Fbxw7}, which promotes ubiquitin-mediated degradation of NICD in a PEST domain-dependent manner (Moretti and Brou, 2013). Herein, we identify a hNICD1-specific degron within the N-terminal region distinct from its C-terminal PEST domain.

RESULTS

NICD1 Is Degraded in *Xenopus* Extract

To recapitulate cytoplasmic NICD turnover, we used the *Xenopus* extract system previously shown to support β-catenin degradation via Wnt pathway components (Chen et al., 2014). In our *Xenopus* extract system, no ongoing transcription or translation confounds our results. We found that radiolabeled in-vitro-translated (IVT) hNICD1 degraded robustly when added to *Xenopus* extract (Figure 1A). Addition of MG132, a proteasome inhibitor, inhibited degradation of both radiolabeled hNICD1 and β-catenin (Figure 1A). Excess recombinant β-catenin inhibited turnover of radiolabeled β-catenin but had no effect on hNICD1 turnover (Figure 1B). Thus, hNICD1 degradation in *Xenopus* extract occurs in a proteasome-dependent manner distinct from that of β-catenin.

NICD Degradation within *Xenopus* Extract Is Restricted to the NICD1 Paralog

In contrast to hNICD1, we found that its paralogs (hNICD2, hNICD3, and hNICD4) were stable throughout the time course

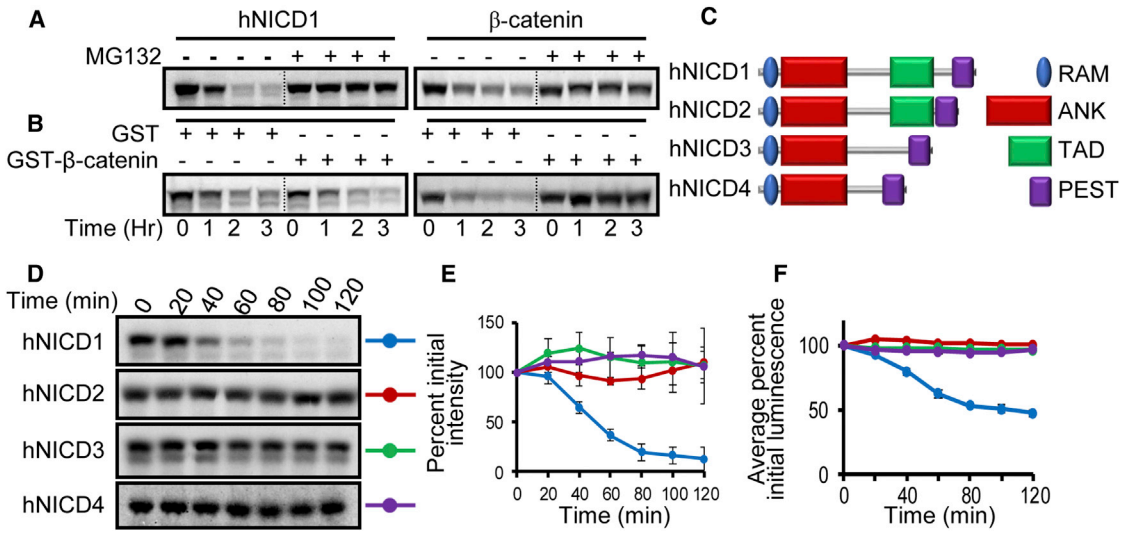

Figure 1. hNICD1 Is Degraded in *Xenopus* Egg Extract

(A) In-vitro-translated (IVT) [^{35}S]hNICD1 and [^{35}S]β-catenin were incubated in extract with DMSO (–) or MG132 (+). Samples were analyzed by SDS-PAGE/autoradiography.

(B) Same as for (A), except extract was supplemented with GST or GST-β-catenin.

(C) Schematic of human NICD paralogs. RAM, RBP-Jκ-associated module domain; ANK, ankyrin repeats domain; TAD, transcriptional activation domain; PEST is proline-, glutamic-acid-, serine-, and threonine-rich region.

(D) Radiolabeled hNICD paralogs were incubated in extract, and samples were removed at the indicated times for SDS-PAGE/autoradiography.

(E) Graph of mean ± SD densitometry measurements for autoradiography experiments.

(F) Degradation of IVT hNICD luciferase fusions incubated in extract parallels degradation of radiolabeled, untagged versions. Graph is mean luciferase signal for two independent experiments (performed in triplicate) and normalized to initial time point (100%).

See also Figure S1.

of our experiment (Figure 1C–1E). To quantify the degradation of NICD proteins in *Xenopus* extract, hNICD paralogs were fused at their C-terminal ends to firefly luciferase (Chen et al., 2014). Although a high background signal is caused by use of internal translational start sites (Chen et al., 2014), the hNICD1 luciferase fusion had a similar half-life as radiolabeled hNICD1 (Figures 1F and S1A). hNICD2, 3, and 4 luciferase fusions were stable, similar to their radiolabeled non-fusion proteins (Figure 1F). This differential degradation was conserved for mouse NICD1 and NICD4 (Figure S1B). We found that the single *Drosophila* NICD ortholog was stable in *Xenopus* extract (Figure S1B).

The N-terminal End of hNICD1 Contains a Degron Required for Degradation in *Xenopus* Extract

Next, we assessed the turnover rates of NICD proteins in *Xenopus* extract versus cultured human cells. We found that NICD-MYC fusions had turnover rates essentially identical to those of their non-tagged versions in extract (Figure S1C). In contrast, all NICD paralogs degraded at similar rates in cultured human cells (Figure S1D), consistent with previous reports (Fryer et al., 2004; Malyukova et al., 2007; Mo et al., 2007; Palermo et al., 2012; Tsunematsu et al., 2004).

The degradation differences between *Xenopus* extract and cultured cells suggest that an uncharacterized degron exists in mammalian NICD1 mechanistically uncoupled in *Xenopus* extract. To identify the NICD1-specific degron, we generated chimeric proteins in which N-terminal or C-terminal portions of hNICD1 were swapped with corresponding portions of other hNICD paralogs (Figures S1E–S1L). These results identified the N terminus of hNICD1 as necessary for its instability within *Xenopus* extract. To narrow the N-terminal portion of hNICD1 responsible for degradation, smaller corresponding swaps of hNICD2 were made with hNICD1 (Figure 2A). We found that the N-terminal 35-amino-acid fragment of hNICD1 was sufficient to confer degradation of hNICD2 (Figures 2B and S1E–S1L). These results show that the amino terminus of hNICD1 contains a Notch1-specific degron (N1-Box) necessary and sufficient to degrade hNICD1 in *Xenopus* extract.

The N-terminal ends of the human NICD paralogs (Figure 2C) contain non-conserved residues within the first 35 amino acids of hNICD1 (residues 1754–1788 of Notch1) that may mediate its degradation. To test this possibility, we mutated these residues to the corresponding hNICD2 residues. In contrast to wild-type hNICD1, the L1755Δ, S1757M, and Q1763K single mutants and triple-mutant hNICD1^{LSQ} were stable in extract (Figures 2D, 2E, and S2A). hNICD1$^{NT\Delta10}$, which lacks the N-terminal ten residues of hNICD1, was also stable in extract, confirming the importance of this region in mediating hNICD1 stability (Figure S2A). All five mutant proteins tested could activate a HES1-luciferase reporter, indicating that they were not grossly misfolded (Figures 2F and 2H). Furthermore, the stabilized mutants demonstrated enhanced reporter activity. The Q1766S mutant demonstrated a slight increased stability in *Xenopus* extract, although Hes1-Luc activation was similar to wild-type. This may reflect subtle differences between *Xenopus* extracts and mammalian cultured cells.

To assess whether the N-terminal region of hNICD1 could promote protein turnover in an autonomous fashion, we fused the N-terminal 50 residues of hNICD1 to luciferase. In contrast to luciferase, hNICD1(1-50)-Luc degraded in extract (Figure S2B). The analogous N1-Box mutants (L1755, S1757, and Q1763) in the hNICD1(1-50)-Luc fusion were stable in *Xenopus* extract (Figure S2B). Next, we altered the first ten residues of NICD2 to those corresponding to NICD1. We found that the chimera, NICD1/2^{NT10}, did not have an increased rate of degradation when compared to wild-type NICD2 (Figure S2C). Enhanced degradation of NICD2, however, was observed on addition of the N-terminal 35 amino acids of NICD1 (Figure S2C). Thus, the N-terminal 35 amino acids of NICD1 constitute the minimal transferable element capable of promoting degradation of the Notch intracellular domain in *Xenopus* extract.

Next, we tested whether N1-Box-regulated degradation of hNICD1 functioned in cultured cells. The N1-Box mutants hNICD1$^{NT\Delta10}$ and hNICD1^{LSQ} were expressed in HEK293 cells, and protein levels assessed by immunoblotting (Figure 2G). Both mutant proteins had higher steady-state levels than did wild-type hNICD1 (Figures 2G and S3A). Consistent with their increased stability, both hNICD1$^{NT\Delta10}$ and hNICD1^{LSQ} had enhanced transcriptional activity (Figure 2H). To test autonomous function of the hNICD1 N1-Box in human cells, we fused the N1-Box to GFP and monitoring turnover by live-cell imaging. In contrast to GFP, hNICD1(1-50)-GFP showed loss of fluorescence at a rate similar to that of full-length hNICD1-GFP (Figures S2D and S2E). A N1-Box double mutant (hNICD1(1-50)^{LS}-GFP) and GFP fusions of the first 50 residues of hNICD2 and 3 did not exhibit substantial turnover (Figure S2E). These results suggest the degradation machinery for the N1-Box of hNICD1 is evolutionarily conserved. We observed turnover of the N1-Box GFP fusion in both the nucleus and cytoplasm, suggesting that N1-Box-mediated degradation could occur in both compartments.

The N1-Box Controls hNICD1 Stability and Activity In Vivo

To ensure that the N1-Box functioned in the complete Notch1 receptor, and to further demonstrate evolutionary conservation, we generated the analogous N1-Box mutant in full-length mouse Notch1 (mNotch1^{LSQ}). Consistent with our hNICD1 studies, mNotch1^{LSQ} exhibited elevated Notch transcriptional activity compared to wild-type mNotch1 (Figure S3B).

To demonstrate that the N1-Box regulates Notch1 function in vivo, we assessed its effects on somite formation in zebrafish embryos. Notch1 plays a role in vertebrate somitogenesis (Harima and Kageyama, 2013; Lewis et al., 2009), and misregulation of Notch signaling during development results in disruption of the symmetric, bilateral somites (Figure 3A). This biological readout was dose sensitive (Figure 3B). Consistent with a role for N1-Box in vivo, injecting mRNA of the N1-Box mutant, *mNotch1*^{LSQ}, caused defective somite formation in nearly double that of *mNotch1* mRNA injected emybros (Figure 3B). It is possible that the enhanced activity of the NICD1 N1-Box mutant is due to its more efficient processing. A mutation in the HD domain of human Notch1 (L1601P) resulted in a constitutively activated "leaky" Notch1 receptor due to its constitutive cleavage from the plasma membrane (Chiang et al., 2006; Thompson et al., 2007; Weng et al., 2004). When combined, the mNotch1$^{L1601P;LSQ}$ mutant had an additive defect in somitogenesis (Figure 3B). These results suggest that the greater activity of the Notch1^{LSQ} is due to increased stability and not more efficient processing.

Inhibition of neural differentiation is a major role of Notch signaling during development. Using the transgenic zebrafish line, Tg(NGN1:GFP), which expresses GFP controlled by the *neurogenin1* (*ngn1*) promoter (marks primary neurons) (Blader et al., 2003), we found that injection of *mNotch1* mRNA decreases the normal *ngn1* expression along the rostral-caudal axis (particularly in the hindbrain) (Figures 3C and S3C). mNotch1^{LSQ} led to a severe decrease in expression of GFP, consistent with its more potent activity. In contrast, injection of *mNotch1* mRNA into Tg(Her4:dRFP), a zebrafish line that expresses RFP under control of the promoter for *her4*, a Notch target gene (Yeo et al., 2007), enhanced RFP expression throughout the central nervous system (Figures 3C and S3C). The expression of RFP was further enhanced (extended caudally) when *mNotch1*^{LSQ} mRNA was injected.

Mutations within the N1-Box Found in Human Tumors Inhibit hNICD1 Degradation

Using the NIH Catalog of Somatic Mutations in Cancer database, we identified two mutations (R1758S and S1776C) in patient tumors located within the first N-terminal 35 residues of hNICD1 (Figure 3D). We found that both mutants exhibit elevated Notch transcriptional activity and steady-state protein levels (Figures 3E and 3F). These mutants also have enhanced activity in vivo as indicated by significantly greater somitogenesis defects on injection of their mRNAs into zebrafish embryos (Figure 3G).

To demonstrate physiologically relevance, we generated transgenic zebrafish encoding the human mutations in the corresponding positions of endogenous zebrafish Notch1 by CRISPR/Cas9-mediated knockin. For all embryos, we performed PCR followed by sequencing to confirm the absence or presence of mutations. We found that all embryos harboring R1758S or S1776C exhibited disrupted somitogenesis (Figure 3H). In contrast, embryos with the wild-type phenotype did not harbor mutant sequences. As control, transgenic animals harboring silent mutations within the N1-Box were generated. We found that none of silent N1-Box mutants exhibited defects in somitogenesis. Transgenic R1758S and S1776C animals demonstrated decreased GFP expression from the *ngn1* promoter and enhanced RFP expression from the *her4* promoter (Figures 3I–3L), consistent with enhanced Notch1 signaling. These changes are not due to gross disruption in embryonic structures (Figures S3D and S3E). No changes in GFP or RFP expression were observed for the control silent mutant embryos. These studies provide strong evidence for an in vivo role of the N1-Box in regulating Notch1 signaling.

The N1-Box Facilitates hNICD1 Degradation Independent of Other *cis* Stability Elements

Two *cis* elements have been identified within the NICD PEST domain that facilitate turnover: the LTPSPE sequence recognized by the SCF^{Fbxw7} complex (Fryer et al., 2002, 2004; O'Neil et al., 2007; Thompson et al., 2007) and the WSSSSP sequence (Chiang et al., 2006). We tested the relative contributions of these

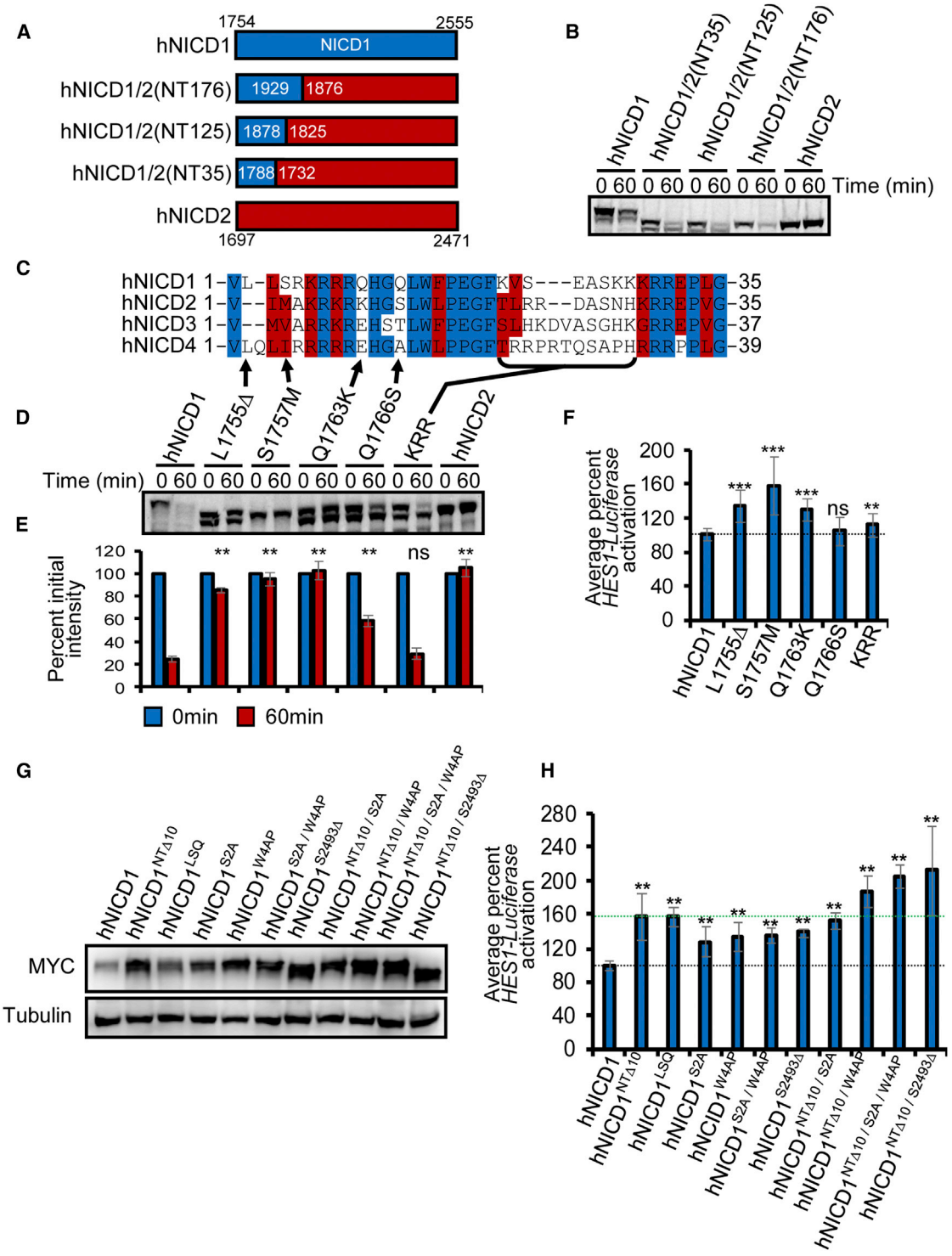

Figure 2. Mutation of N1-Box Inhibits hNICD1 Degradation in *Xenopus* Egg Extract and Elevates Steady-State Levels and Transcriptional Activity in Cultured Human Cells

(A) Schematic of hNICD1 and hNICD2 chimeras. Parentheses indicate the number of N-terminal residues of hNICD1 in each chimera.

(B) Radiolabeled hNICD1/2 chimeras containing at least the N-terminal 35 residues of hNICD1 degraded robustly in *Xenopus* egg extract.

(C) Alignment of N-terminal regions of human NICD paralogs.

(legend continued on next page)

two elements and the N1-Box to NICD1 stability. Consistent with previous studies, mutation of LTPSPE (S2514A/S2517A; hNICD1^{S2A}), WSSSSP (hNICD1^{W4AP}), both LTPSPE and WSSSSP (hNICD1$^{S2A/W4AP}$), or truncation of the PEST region (hNICD1$^{S2493\Delta}$) resulted in increased protein levels in cultured cells (Figure 2G) (Chiang et al., 2006; Fryer et al., 2004; O'Neil et al., 2007; Thompson et al., 2007; Weng et al., 2004). Increased steady-state levels of hNICD1^{S2A} and hNICD1^{W4AP} were also observed in combination with NTΔ10. Interestingly, combining hNICD1$^{NT\Delta10}$ with W4AP and/or S2493Δ, but not with S2A, enhanced protein levels. All stabilizing mutants demonstrated enhanced HES1 reporter activation, and protein levels of each hNICD1 mutant roughly correlated with the degree of activation of Notch transcription (Figure 2H). We observed a similar effect in zebrafish embyros in which injected Notch1$^{LSQ/S2647\Delta}$ (S2647Δ is the mouse PEST deletion) was more potent in disrupting somitogenesis (Figure 3B). These results suggest that WSSSSP and the N1-Box act independent of each other. The absence of further activation by hNICD1$^{NT\Delta10}$ or hNICD1^{W4AP} on mutation of the Fbxw7 binding site may indicate that stabilization by NTΔ10 or WSSSSP fully saturates the SCF^{Fbxw7} complex, which may be limiting.

The N1-Box Is Not Regulated by Fbxw7 or Itch

In addition to known *cis* factors, we also assessed whether two known NICD E3 ubiquitin ligases contributed to N1-Box-mediated degradation. We overexpressed Fbxw7 and a dominant-negative form (Fbxw7DN) (Skaar et al., 2013; Wu et al., 2001). As previously reported, overexpression of Fbxw7 decreased, and Fbxw7DN increased, steady-state levels of hNICD1 (Figure S4A) (Gupta-Rossi et al., 2001; Wu et al., 2001). In contrast, overexpressing Fbxw7 or Fbxw7DN did not affect levels of the Fbxw7 binding site mutant, hNICD1^{S2A} (Figure S4A). The effects of overexpressing Fbxw7 and Fbxw7DN on wild-type hNICD1 were similarly observed for hNICD1^{W4AP} (Figure S4A), consistent with our results and a previous study suggesting that WSSSSP acts independent of the SCF^{Fbxw7} complex (Chiang et al., 2006). A similar effect was observed for NICD1$^{NT\Delta10}$, indicating that the N1-Box mediates degradation of NICD1 independent of the SCF^{Fbxw7} complex.

All NICD paralogs contain a C-terminal PEST domain recognized by the SCF^{Fbxw7} ubiquitin ligase (Gupta-Rossi et al., 2001; Moretti and Brou, 2013; Oberg et al., 2001; Wu et al., 2001). The Fbxw7 isoform shown to ubiquitinate NICD proteins is localized to the nucleus (O'Neil et al., 2007). In support of this, we could not detect Fbxw7 by immunoblotting *Xenopus* extract, which does not contain nuclei (Figure S4B). In addition, two Fbxw7 binding mutants hNICD1^{S3A} and hNICD$^{S2493\Delta}$ degraded at rates indistinguishable from that of wild-type hNICD1 (Figures S4C–S4F). Thus, the incapacity of extract to degrade NICD2-4 is likely due to the absence of Fbxw7, and NICD1 degradation in *Xenopus* extract does not require its PEST domain or Fbxw7.

The E3 ligase, Itch, promotes PEST domain-independent NICD1 degradation (Qiu et al., 2000). As previously shown, overexpression of Itch decreased, whereas overexpression of a dominant-negative form, Itch^{C380A}, increased, hNICD1 steady-state levels in HEK293 cells (Figure S4G). We obtained similar results for all of our mutants, indicating that Itch does not mediate NICD1 degradation through the N1-Box.

hNICD1 Turnover Is Inhibited by CSL

Based on sequence overlap between the N1-Box and RAM domain (the major *cis* factor involved in CSL binding (Nam et al., 2003; Tamura et al., 1995) (Figure 4A), we tested whether binding of CSL to hNICD1 could influence hNICD1 stability. Given the cytoplasmic nature of *Xenopus* egg extract (lacks nuclei), it likely contains low levels of CSL. Incubation of recombinant CSL with *Xenopus* extract inhibited hNICD1 degradation in a dose-dependent manner (Figures 4B and 4C). Inhibition of hNICD1 degradation by CSL requires direct binding because degradation of hNICD1$^{1771\text{-}74A}$, which cannot bind CSL (Chu and Bresnick, 2004; Vasquez-Del Carpio et al., 2011), is not inhibited by recombinant CSL (Figures 4B and 4C). In cultured human cells, where CSL is present, we predicted that hNICD1$^{1771\text{-}74A}$ would be less stable than wild-type hNICD1. In support of this idea, we observed lower steady-state levels of hNICD1$^{1771\text{-}74A}$ than for wild-type hNICD1 when expressed in HEK293 cells (Figures 4D and 4E).

Degradation of NICD via the SCF^{Fbxw7}/PEST domain depends on assembly of a CSL transcriptional complex (Fryer et al., 2002, 2004). We predicted that hNICD1$^{1771\text{-}74A}$ instability is primarily mediated by the N1-Box. Thus, an N1-Box/CSL-binding double mutant should be more stable than the N1-Box mutant, and a hNICD1 PEST/CSL binding double mutant should be less stable than a PEST domain mutant due to enhanced N1-Box-mediated degradation. Consistent with this idea, we found that hNICD1$^{NT\Delta10/1771\text{-}74A}$ steady-state levels are statistically higher than those of hNICD1$^{NT\Delta10}$ and that hNICD1$^{1771\text{-}74A\ /\ S2493\Delta}$ steady-state levels are lower than those of hNICD1$^{S2493\Delta}$

(D) Mutation of hNICD1 non-conserved residues at position L1755, S1757, or Q1763 inhibits degradation in extract. Δ, amino acid deletion; KRR, lysine-rich region. Intervening lanes were removed. The lower bands observed in (B) and (D) represent an internal translational initiation product (thus are missing an N-terminal fragment) resistant to degradation (Chen et al., 2014).

(E) Mean ± SD quantification of densitometry for experiments represented in (D). Data are from three independent experiments. $^{**}p < 0.05$; ns, not significant.

(F) N-terminal mutants of hNICD1 are transcriptionally active as assessed by HES1-luciferase Notch reporter activity in HEK293 cells. Luciferase activity was measured after 24 hr. Graph represents ± SD of luciferase signal normalized to *Renilla* luciferase of at least three independent experiments (performed in triplicate). $^{***}p < 0.0001$, $^{**}p < 0.05$ relative to hNCID1. ns, not significant.

(G) N1-Box mutants (hNICD$^{NT\Delta10}$ and hNICD^{LSQ}), Fbxw7 binding mutant (hNICD1^{S2A}), WSSSSP mutant (hNICD1^{W4AP}), or combinations were expressed in HEK293 cells, and immunoblotting of lysates was performed. Tubulin was used as a control.

(H) Stabilizing hNICD1 N1-Box mutants, Fbxw7, and WSSSP exhibit higher transcriptional activity than does hNICD1 as assessed by HES1-luciferase reporter activity in HEK293 cells. Luciferase activity was measured after 24 hr. Graphs show mean ± SD of the luciferase signal normalized to *Renilla* luciferase of at least two independent experiments (performed in triplicate). $^{**}p < 0.002$ relative to hNICD1.

See also Figures S2, S3, and S4.

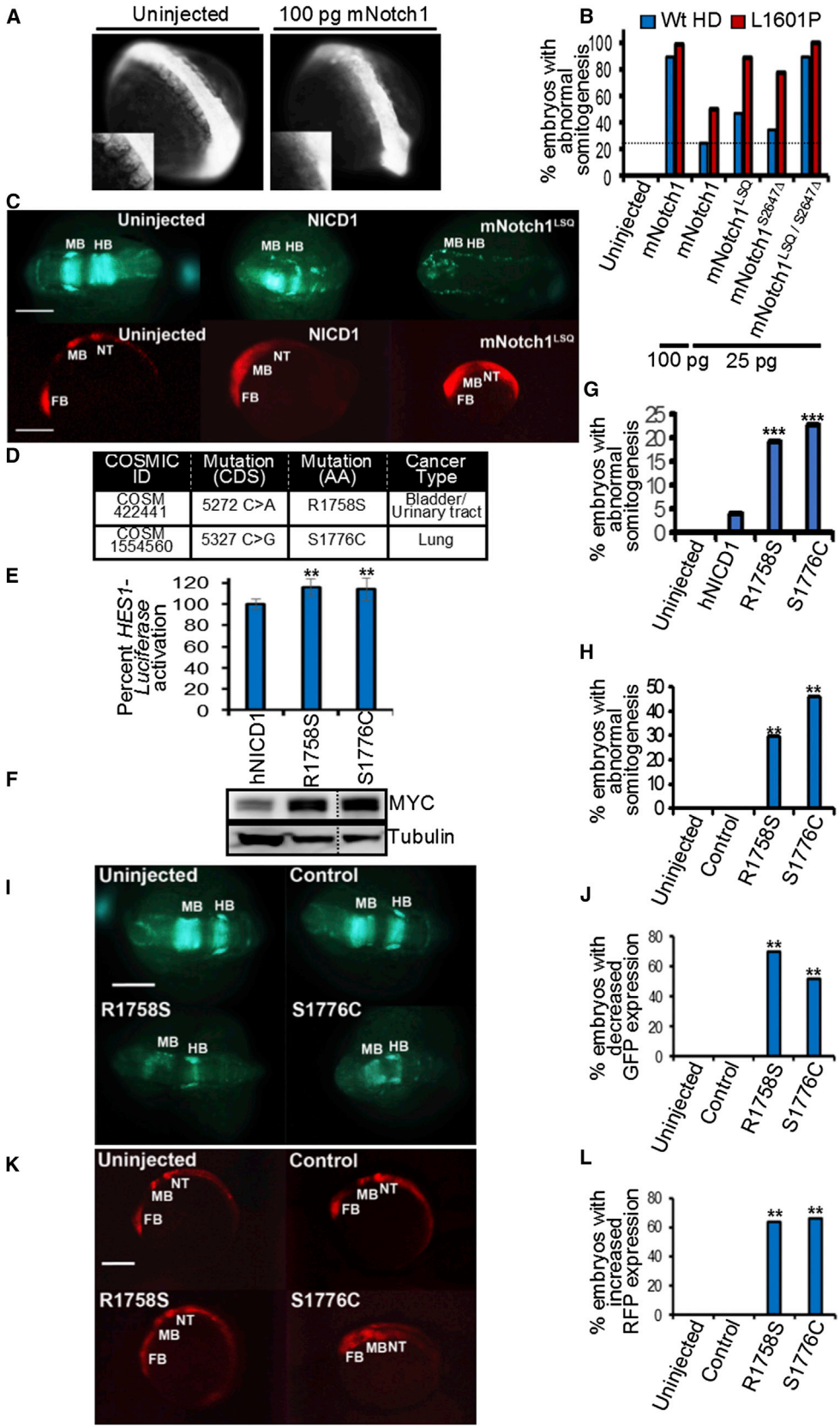

(legend on next page)

(Figures 4D and 4E). These results suggest that CSL binding to NICD1 inhibits its turnover by blocking N1-Box-mediated degradation.

DISCUSSION

Evidence for an in vivo role of the N1-Box comes from a previous report showing that a chimeric receptor containing the Notch2 extracellular domain and Notch1 intracellular domain (Notch21) is 2-fold more active than is a wild-type Notch1 when expressed at similar levels in mice (Liu et al., 2013). Interestingly, the Notch21 chimeric fusion deleted the N1-Box of NICD1. Our data suggest that increased activity of this chimera is due to increased stability of its intracellular domain. We propose a model (Figure 4F) in which liberated NICD1 (on cleavage from the Notch1 receptor) has two possible fates: (1) rapid degradation and inactivation via its N1-Box or (2) binding to CSL and Notch transcriptional complex components to drive Notch target gene transcription. Termination of Notch1 signaling occurs on ubiquitin-mediated degradation by the SCF^{Fbxw7}/proteasome.

It is not as clear why a cell needs to regulate cytoplasmic NICD1 degradation. One possibility is that this system dampens stochastic flux in the system, thereby minimizing noise: a threshold level of Notch receptor activation must occur for activation of transcription. Indeed, recent models of juxtacrine signaling indicate that such systems are inherently noisy (Yaron et al., 2014). This may explain why *Drosophila* NICD does not have an N1-Box, as stochastic flux in Notch signaling plays an important role during neuroblast differentiation via lateral inhibition (Artavanis-Tsakonas et al., 1999). Conversely, once the transcriptional complex is fully saturated (i.e., all CSL is occupied by NICD1), unbound NICD1 could be degraded to limit the activation window. This model is consistent with the digital response model proposed for Notch1 pathway activation (Ilagan et al., 2011).

We favor a model in which N1-Box mutants stabilize NICD1 protein by directly disrupting the interaction of NICD1 with an as yet unknown E3 ligase. Because the N1-Box and the RAM domains overlap, however, it is possible that certain cancer mutations may enhance NICD1-CSL interaction and indirectly block the action of the E3 ligase. Activating mutations in Notch have been found in a large percentage of T-ALL cases. To date, we have not found N1-Box mutations in T-ALL. It is possible that T cells have other mechanisms to control cytoplasmic levels of NICD1. Alternatively, turnover by other E3 ligases (e.g., Fbxw7 and/or Itch) may be the predominant mechanism by which cytoplasmic NICD1 levels are regulated.

EXPERIMENTAL PROCEDURES

Animals

All *Xenopus laevis* and zebrafish studies were approved by the Vanderbilt University Institutional Animal Care and Use Committee and were performed in accordance with institutional and federal guidelines. See Supplemental Information for more details.

Cell Culture

HEK293 cells were maintained in DMEM (Corning) supplemented with 1% L-glutamine, 10% (v/v) fetal bovine serum, 100 μg/ml streptomycin, and 100 U/ml penicillin at 37°C with 5% CO_2. Transient transfections were performed using Fugene HD (Promega) in accordance with the manufacturer's

Figure 3. Notch1 N1-Box Mutants Found in Human Cancers Have Increased Activity in Cultured Human Cell and Zebrafish Embryos

(A) The N1-Box Notch1 mutant exhibits enhanced capacity to disrupt somitogenesis in embryos. Representative images of 10–13 somite stage zebrafish embryos, uninjected and injected (100 pg of *mNotch1* mRNA). Inset is higher magnification.

(B) Quantification of zebrafish embryos (10–13 somite stage) with defective somites. Data are from three clutches collected from three different breeding pairs per clutch. n = 78–200 embryos per injection. **$p < 0.05$ relative to 25 pg *Notch1* mRNA injection. ***$p < 0.005$ relative to 25 pg $hNICD1^{LSQ;\ S2467\Delta}$ mRNA injection, except for comparison to *Notch1* 100 pg injection (not significant).

(C) (Top) Injection into the zebrafish line, Tg[NGN1:GFP], that expresses GFP in primary neurons under control of the *ngn1* promoter. Coronal views of embryos at 8× magnification. Embryos with reduced GFP expression: uninjected = 0/44, mNotch1 = 24/32, and $mNotch1^{LSQ}$ = 17/40. Injection of 25 pg. (Bottom) Injection into the zebrafish line, Tg[Her4:dRFP], that expresses RFP under the control of the *her4* Notch target gene promoter. Sagittal view of embryos (14 hpf) at 5× magnification. Data are from at least three clutches collected from three different breeding pairs. Embryos with increased RFP expression: uninjected = 0/75, mNotch1 = 60/68, and $mNotch1^{LSQ}$ = 45/53. Injection of 25 pg. Hpf is14 hr post-fertilization. Scale bar, 0.3 mm.

(D) Table of somatic mutations found within residues 1754–1788 of hNotch1 (residues 1–35 of hNICD1) from the COSMIC database.

(E) Human cancer mutants in the N1-Box expressed in HEK293 cells show elevated HES1-luciferase reporter activity. Graph shows mean ± SD of the luciferase signal normalized to *Renilla* luciferase of at least three independent experiments performed in triplicate. **$p \leq 0.007$ relative to hNICD1.

(F) hNotch1 R1758S and S1776C mutants expressed in cultured cells have elevated steady-state levels. Tubulin was used as a loading control. Intervening lanes were removed.

(G) Quantification of 10–13 somite stage zebrafish embryos with defective somites (injected with 50 pg of indicated mRNA). Data are from at least three clutches collected from three different breeding pairs. n = 30–320 embryos per injection. ***$p < 0.0005$ relative to hNICD1.

(H) Zebrafish embryos were injected with Cas9 nuclease mRNA, short guide RNA, and donor single-strand oligonucleotides encoding R1758S, S1776C, or Notch1 silent mutation (control). Transgenics expressing the R1758S or S1776C mutation in zebrafish Notch1 exhibit defects in somite formation. In contrast, no somitogenesis defects are observed in transgenics harboring silent mutations of zebrafish Notch1. Graph shows quantification of zebrafish embryos (10–13 somite stage) with defective somites. Number of embryos: uninjected = 210, control = 70, S1776C = 165, and R1758S = 189.

(I–L) R1758S and S1776C transgenic mutants exhibit decreased GFP (I) and increased RFP (K) expression in the Tg[NGN1:GFP] and Tg[Her4:dRFP] lines, respectively, when compared to uninjected and Notch1 silent mutant embryos. For Tg[NGN1:GFP] transgenics, coronal views are shown at 8× magnification. Embryos with reduced GFP expression: uninjected = 0/75, control = 0/44, R1758S = 28/40, and S1776C = 16/31. For Tg[Her4:dRFP] transgenics, sagittal views are shown at 5× magnification. Embryos with enhanced RFP expression: uninjected = 0/75, control = 0/30, R1758S = 36/57, and S1776C = 49/74. **$p < 0.005$ relative to control injected embryos. Scale bar, 0.3 mm. For (J) and (L), graphs show quantification of zebrafish embryos with reduced GFP (J) or enhanced RFP expression (L). Sequencing confirms the presence of the mutations for all affected embryos and the absence of amino acid changes for all non-affected animals. Embryos are 14 hr post-fertilization. FB, forebrain; MB, midbrain; HB, hindbrain; NT, neural tube.

See also Figure S3.

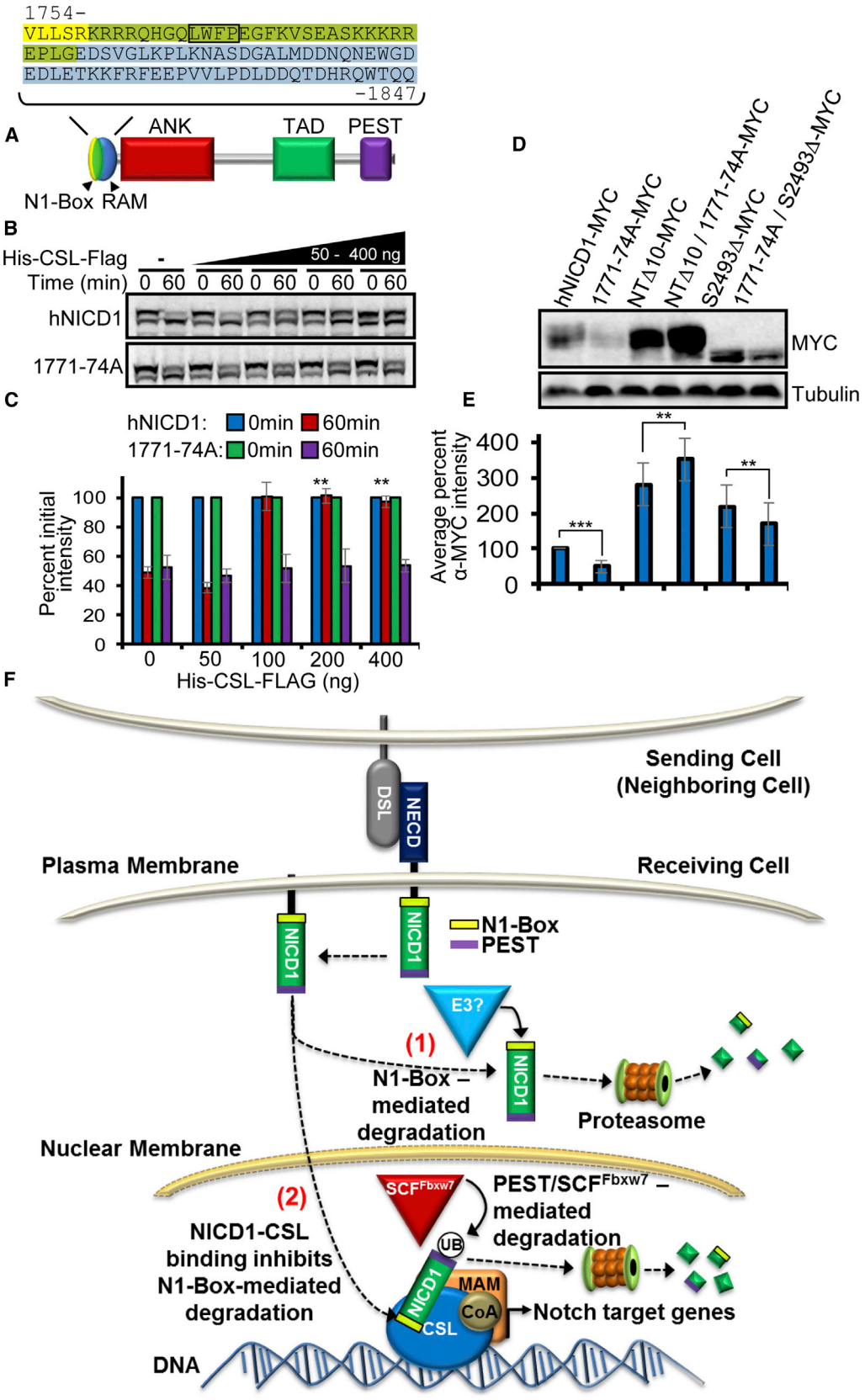

(legend on next page)

suggestions. For cyclohexamide (Sigma-Alderich) chase experiments, media supplemented with 100 μg/ml cyclohexamide was added to cells at the 0 min time point. Cells were then incubated in the presence of cyclohexamide for the duration of the experiment.

Transcriptional Activity Assays

HEK293 cells were transiently transfected with 1 μg Hes1-luciferase, 0.5 μg Renilla luciferase, and 1 μg of the indicated Notch construct. Luciferase and Renilla activities were assessed after 24 hr using the Dual-Glo Luciferase Assay System (Promega) in accordance with the manufacturer's instructions. Experiments were performed in triplicate and replicated at least two times. Significance was determined using a two-tailed Student's t test.

Xenopus Egg Extract Degradation Assays

Detailed methodology for preparing *Xenopus* egg extract and performing degradation assays with radiolabeled and luciferase fusion proteins can be found in Chen et al. (2014). His-CSL-Flag was purified from SF21 cells as previously described (Vasquez-Del Carpio et al., 2011). Glutathione S-transferase (GST)-β-catenin (gift from Wenqing Xu) was expressed and purified from bacterial cell lysates with glutathione beads (Merck Millipore) in accordance with the manufacturer's suggestions.

Immunoblot Analysis

To assess changes in steady-state protein levels, 1 μg of each DNA construct was transfected into an equivalent number of HEK293 cells. 48 hr post-transfection, cells were lysed by incubation in non-denaturing lysis buffer (50 mM Tris-HCl [pH 7.4], 300 mM NaCl, 5 mM EDTA, 1% (w/v) Trition X-100, and 1 mM PMSF) for 30 min on ice. Lysates were rigorously vortexed once at 15 min during the incubation. Lysates were cleared by centrifugation. 50 μg of total protein, assessed using the Bio-Rad protein assay dye reagent (Bio-Rad), was processed for SDS-PAGE/immunoblotting using standard techniques. The following antibodies were used: α-Fbxw7 (Bethyl Laboratories, Cat# A301-720A), α-MYC (9E10), α-Flag (Sigma-Aldrich), and α-β-tubulin (Clone E7, Developmental Studies Hybridoma Bank, University of Iowa). Secondary antibodies conjugated to horseradish peroxidase were purchased from Bethyl Laboratories. Blots were analyzed using ImageJ software.

Statistical Methods

Luciferase fusion degradation experiments were repeated at least twice and in triplicate. Significance was calculated using a two-tailed Student's t test in Excel. Transcriptional assays were performed in triplicate and replicated at least two times. Significance was determined using a two-tailed Student's t test. Autoradiography, immunoblots, and fluoresence microscopy experiments were analyzed using ImageJ software and significance (two-tailed Student's t test) was calculated in Excel. Somite formation assays were assessed using Fisher's exact test calculated in Excel.

Additional experimental methods are provided within the Supplemental Experimental Procedures.

SUPPLEMENTAL INFORMATION

Supplemental Information includes Supplemental Experimental Procedures and four figures and can be found with this article online at http://dx.doi.org/10.1016/j.celrep.2016.04.070.

AUTHOR CONTRIBUTIONS

M.R.B. conceived of, designed, executed, and interpreted the experiments. T.W.C. designed and executed experiments and provided intellectual input. J.N.J. performed microscopy-based turnover studies. L.R.N. performed zebrafish experiments. J.G.P. provided expertise on zebrafish. L.A.L. provided intellectual input and final manuscript editing. A.S. provided reagents and intellectual input. D.J.R. and A.J.C. provided Flag-CSL-His protein and intellectual input. E.L. and S.S.H. provided intellectual guidance and reagents. M.R.B., S.S.H., and E.L. wrote the manuscript.

ACKNOWLEDGMENTS

The authors thank A. Marchese, R. Deshaies, R. Kopan, and DNASU for reagents and members of the E.L. lab for helpful discussions. The authors also thank Q. Guan for help with zebrafish husbandry. M.R.B. was supported by a National Cancer Institute training grant (T32 CA119925). T.W.C. was supported by an American Heart Association predoctoral fellowship (12PRE6590007). L.R.N. was supported by the Training Program in Stem Cell and Regenerative Developmental Biology (T32 HD007502). V.H.N. was supported by the Microenvironment Influences in Cancer Training Grant (T32 CA00959228). J.G.P. and S.S.H. were supported by the NIH (RO1 EY024354 and R01DK078640, respectively). A.S. was supported by the NIH (RO1GM092924 and RO1GM110041). A.J.C. was supported by the National Cancer Institute (NCI R01CA083736-12A1 and NCI R01CA125044-02). E.L. was supported by the NIH (R01GM081635, R01GM103926, and P30 CA068485).

Received: October 27, 2014
Revised: March 14, 2016
Accepted: April 19, 2016
Published: May 19, 2016

REFERENCES

Artavanis-Tsakonas, S., Rand, M.D., and Lake, R.J. (1999). Notch signaling: cell fate control and signal integration in development. Science *284*, 770–776.

Blader, P., Plessy, C., and Strähle, U. (2003). Multiple regulatory elements with spatially and temporally distinct activities control neurogenin1 expression in primary neurons of the zebrafish embryo. Mech. Dev. *120*, 211–218.

Chen, T.W., Broadus, M.R., Huppert, S.S., and Lee, E. (2014). Reconstitution of β-catenin degradation in Xenopus egg extract. J. Vis. Exp. (*88*)

Chiang, M.Y., Xu, M.L., Histen, G., Shestova, O., Roy, M., Nam, Y., Blacklow, S.C., Sacks, D.B., Pear, W.S., and Aster, J.C. (2006). Identification of a conserved negative regulatory sequence that influences the leukemogenic activity of NOTCH1. Mol. Cell. Biol. *26*, 6261–6271.

Chu, J., and Bresnick, E.H. (2004). Evidence that C promoter-binding factor 1 binding is required for Notch-1-mediated repression of activator protein-1. J. Biol. Chem. *279*, 12337–12345.

Fryer, C.J., Lamar, E., Turbachova, I., Kintner, C., and Jones, K.A. (2002). Mastermind mediates chromatin-specific transcription and turnover of the Notch enhancer complex. Genes Dev. *16*, 1397–1411.

Figure 4. N1-Box-Mediated hNICD1 Degradation in *Xenopus* Egg Extract and Cultured Human Cells Is Inhibited by Its Binding to CSL

(A) Schematic showing overlap of N1-Box (yellow) and RAM domains (blue). Overlapping sequence is displayed in green. A black box outlines the ΦWΦP motif.

(B) CSL inhibits degradation of hNICD1 (but not a CSL binding mutant) in a dose-dependent manner. Radiolabeled hNICD1 or hNICD$^{11771\text{-}74A}$ was incubated in *Xenopus* egg extract with increasing amounts of recombinant CSL. Samples were removed after 1 hr and subjected to SDS-PAGE/autoradiography.

(C) Graph shows the mean ± SD of densitometry measurements for two independent experiments represented in (B). $^{**}p < 0.05$.

(D) Steady-state levels of the CSL binding mutant, hNICD1$^{11771\text{-}74A}$, are lower than hNICD1 in cultured cells. Plasmids encoding indicated N1-Box and CSL binding mutants were transfected into HEK293 cells and immunoblotting performed. Tubulin was used as a loading control.

(E) Graph of densitometry measurements in (D). Graph shows mean ± SD of MYC intensities normalized to tubulin for six independent experiments. $^{**}p < 0.05$, $^{***}p \leq 0.001$.

(F) Model of N1-Box-mediated regulation of hNotch1 signaling. See text for details.

See also Figure S4.

Fryer, C.J., White, J.B., and Jones, K.A. (2004). Mastermind recruits CycC:CDK8 to phosphorylate the Notch ICD and coordinate activation with turnover. Mol. Cell *16*, 509–520.

Gupta-Rossi, N., Le Bail, O., Gonen, H., Brou, C., Logeat, F., Six, E., Ciechanover, A., and Israël, A. (2001). Functional interaction between SEL-10, an F-box protein, and the nuclear form of activated Notch1 receptor. J. Biol. Chem. *276*, 34371–34378.

Harima, Y., and Kageyama, R. (2013). Oscillatory links of Fgf signaling and Hes7 in the segmentation clock. Curr. Opin. Genet. Dev. *23*, 484–490.

Ilagan, M.X., Lim, S., Fulbright, M., Piwnica-Worms, D., and Kopan, R. (2011). Real-time imaging of notch activation with a luciferase complementation-based reporter. Sci. Signal. *4*, rs7.

Kopan, R., and Ilagan, M.X. (2009). The canonical Notch signaling pathway: unfolding the activation mechanism. Cell *137*, 216–233.

Kovall, R.A., and Blacklow, S.C. (2010). Mechanistic insights into Notch receptor signaling from structural and biochemical studies. Curr. Top. Dev. Biol. *92*, 31–71.

Lewis, J., Hanisch, A., and Holder, M. (2009). Notch signaling, the segmentation clock, and the patterning of vertebrate somites. J. Biol. *8*, 44.

Liu, Z., Chen, S., Boyle, S., Zhu, Y., Zhang, A., Piwnica-Worms, D.R., Ilagan, M.X., and Kopan, R. (2013). The extracellular domain of Notch2 increases its cell-surface abundance and ligand responsiveness during kidney development. Dev. Cell *25*, 585–598.

Malyukova, A., Dohda, T., von der Lehr, N., Akhoondi, S., Corcoran, M., Heyman, M., Spruck, C., Grandér, D., Lendahl, U., and Sangfelt, O. (2007). The tumor suppressor gene hCDC4 is frequently mutated in human T-cell acute lymphoblastic leukemia with functional consequences for Notch signaling. Cancer Res. *67*, 5611–5616.

Mo, J.S., Kim, M.Y., Han, S.O., Kim, I.S., Ann, E.J., Lee, K.S., Seo, M.S., Kim, J.Y., Lee, S.C., Park, J.W., et al. (2007). Integrin-linked kinase controls Notch1 signaling by down-regulation of protein stability through Fbw7 ubiquitin ligase. Mol. Cell. Biol. *27*, 5565–5574.

Moretti, J., and Brou, C. (2013). Ubiquitinations in the notch signaling pathway. Int. J. Mol. Sci. *14*, 6359–6381.

Nam, Y., Weng, A.P., Aster, J.C., and Blacklow, S.C. (2003). Structural requirements for assembly of the CSL.intracellular Notch1.Mastermind-like 1 transcriptional activation complex. J. Biol. Chem. *278*, 21232–21239.

O'Neil, J., Grim, J., Strack, P., Rao, S., Tibbitts, D., Winter, C., Hardwick, J., Welcker, M., Meijerink, J.P., Pieters, R., et al. (2007). FBW7 mutations in leukemic cells mediate NOTCH pathway activation and resistance to gamma-secretase inhibitors. J. Exp. Med. *204*, 1813–1824.

Oberg, C., Li, J., Pauley, A., Wolf, E., Gurney, M., and Lendahl, U. (2001). The Notch intracellular domain is ubiquitinated and negatively regulated by the mammalian Sel-10 homolog. J. Biol. Chem. *276*, 35847–35853.

Palermo, R., Checquolo, S., Giovenco, A., Grazioli, P., Kumar, V., Campese, A.F., Giorgi, A., Napolitano, M., Canettieri, G., Ferrara, G., et al. (2012). Acetylation controls Notch3 stability and function in T-cell leukemia. Oncogene *31*, 3807–3817.

Qiu, L., Joazeiro, C., Fang, N., Wang, H.Y., Elly, C., Altman, Y., Fang, D., Hunter, T., and Liu, Y.C. (2000). Recognition and ubiquitination of Notch by Itch, a hect-type E3 ubiquitin ligase. J. Biol. Chem. *275*, 35734–35737.

Skaar, J.R., Pagan, J.K., and Pagano, M. (2013). Mechanisms and function of substrate recruitment by F-box proteins. Nat. Rev. Mol. Cell Biol. *14*, 369–381.

Tamura, K., Taniguchi, Y., Minoguchi, S., Sakai, T., Tun, T., Furukawa, T., and Honjo, T. (1995). Physical interaction between a novel domain of the receptor Notch and the transcription factor RBP-J kappa/Su(H). Curr. Biol. *5*, 1416–1423.

Thompson, B.J., Buonamici, S., Sulis, M.L., Palomero, T., Vilimas, T., Basso, G., Ferrando, A., and Aifantis, I. (2007). The SCFFBW7 ubiquitin ligase complex as a tumor suppressor in T cell leukemia. J. Exp. Med. *204*, 1825–1835.

Tsunematsu, R., Nakayama, K., Oike, Y., Nishiyama, M., Ishida, N., Hatakeyama, S., Bessho, Y., Kageyama, R., Suda, T., and Nakayama, K.I. (2004). Mouse Fbw7/Sel-10/Cdc4 is required for notch degradation during vascular development. J. Biol. Chem. *279*, 9417–9423.

Vasquez-Del Carpio, R., Kaplan, F.M., Weaver, K.L., VanWye, J.D., Alves-Guerra, M.C., Robbins, D.J., and Capobianco, A.J. (2011). Assembly of a Notch transcriptional activation complex requires multimerization. Mol. Cell. Biol. *31*, 1396–1408.

Weng, A.P., Ferrando, A.A., Lee, W., Morris, J.P., 4th, Silverman, L.B., Sanchez-Irizarry, C., Blacklow, S.C., Look, A.T., and Aster, J.C. (2004). Activating mutations of NOTCH1 in human T cell acute lymphoblastic leukemia. Science *306*, 269–271.

Wu, G., Lyapina, S., Das, I., Li, J., Gurney, M., Pauley, A., Chui, I., Deshaies, R.J., and Kitajewski, J. (2001). SEL-10 is an inhibitor of notch signaling that targets notch for ubiquitin-mediated protein degradation. Mol. Cell. Biol. *21*, 7403–7415.

Yaron, T., Cordova, Y., and Sprinzak, D. (2014). Juxtacrine signaling is inherently noisy. Biophys. J. *107*, 2417–2424.

Yeo, S.Y., Kim, M., Kim, H.S., Huh, T.L., and Chitnis, A.B. (2007). Fluorescent protein expression driven by her4 regulatory elements reveals the spatiotemporal pattern of Notch signaling in the nervous system of zebrafish embryos. Dev. Biol. *301*, 555–567.